Talanta 298 (2026) 128923

Contents lists available at ScienceDirect

Talanta

journal homepage: www.elsevier.com/locate/talanta

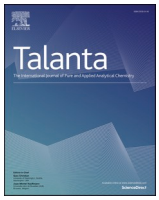

Incorporation of optical profilometry volume correction in quantitative elemental bioimaging workflows

Dayanne Mozaner Bordin [a,*], Thomas Lockwood [a], Mika Westerhausen [a], Janice Irene McCauley [a], Astrid Jeibmann [b], Jessica Chitty [c,d], Thomas Cox [c,d], Philip A. Doble [a]

[a] HyMaS Laboratory, School of Mathematical and Physical Sciences, University of Technology Sydney, Australia
[b] Institute of Neuropathology, University Hospital Münster, Pottkamp 2, 48149, Münster, Germany
[c] Garvan Institute of Medical Research and the Kinghorn Cancer Centre, Darlinghurst, New South Wales, Australia
[d] School of Clinical Medicine, Faculty of Medicine, UNSW Sydney, Kensington, New South Wales, Australia

ARTICLE INFO

Keywords:
LA-ICP-MS
Bioimaging
Optical profilometry
Accuracy
Quantification

ABSTRACT

Quantitative elemental bioimaging workflows are well established and typically rely on matrix-matched standards for comparable and repeatable calibration. However, variations in tissue thickness, microtome cutting artefacts, and cell density are usually assumed to have negligible impact on method uncertainties. Common mitigation strategies include endogenous signal normalization with ^{12}C or ^{31}P, complete ablation of thin sections, or analysis of thicker specimens under stable laser fluences. While effective for homogeneous specimens, these approaches may fail in heterogeneous tissues with disparate anatomical structures, variable cell populations, or inconsistencies in sectioning, leading to uncontrolled anomalies and potentially misleading interpretation of elemental distributions. To overcome these limitations, here we incorporate optical profilometry into quantitative bioimaging workflows to directly measure tissue surface topographies and correct for thickness variations. Topographic maps were acquired for gelatin standards and representative tissues, including murine kidney, multi-organ arrays, human meningioma, and emphysematous lung, revealing substantial deviations from nominal thicknesses and heterogeneous surface roughness. These data were registered against LA-ICP-MS elemental images and applied for volume normalization. Volume correction significantly altered elemental quantification. In kidney, Cu, Fe, and Zn increased 4–5 fold, whereas in meningioma, Cu and Fe increased 8–10 fold, with Zn similarly elevated. Correlations of endogenous signals with thickness were tissue-dependent: in the kidney, ^{12}C strongly correlated ($R = 0.66$) and ^{31}P moderately ($R = 0.44$), while in the meningioma, both were weak (^{12}C $R = 0.21$; ^{31}P $R = 0.09$), though ^{31}P moderately tracked cell density ($R = 0.51$). These results demonstrate that profilometry-based volume correction improves accuracy, reproducibility, and interpretability of elemental bioimaging, particularly in heterogeneous tissues.

1. Introduction

Elemental bioimaging by laser ablation–inductively coupled plasma–mass spectrometry (LA-ICP-MS) for quantification of distributions of elements in biological specimens is of increasing utility in diverse fields of inquiry in medical, biological, clinical, forensic, and environmental sciences [1,2]. Modern LA-ICP-MS instruments and validated analytical workflows have vastly improved acquisition times and sensitivity at cellular and subcellular resolutions [3,4] revealing novel discoveries of the role of elements in biological pathways such as innate host immune responses, intracellular signaling, cancer pathogenesis [5] and human tumor radioresistance [6].

The main challenges for precise and accurate quantification of elements in heterogeneous biological tissues have been largely overcome by preparation of matrix-matched standards that replicate biological tissues' physical and chemical properties, or gelatin-based standards [7,8]. However, variations of specimen thickness, cutting artefacts, disparate tissue domains and density, are either ignored, presumed to be non-significant contributors to method statistical uncertainties, or partially mitigated using several approaches. For example, total

* Corresponding author.
E-mail address: Dayanne.Bordin@uts.edu.au (D. Mozaner Bordin).

https://doi.org/10.1016/j.talanta.2025.128923
Received 1 July 2025; Received in revised form 24 September 2025; Accepted 28 September 2025
Available online 29 September 2025

consumption of thin precisely cut biological specimens assume thickness and ablation volume uniformity. However, this method is not viable for routine analyses of tissues where sectioning is not controlled, or when samples are obtained from different sources.

Alternatively, analyses of thicker sections require stable and consistent laser power for the duration of a single analysis, and for longitudinal or extended studies. This requirement is not practicable as power variability cannot be adequately controlled due to inherent limitations of laser technology. In such cases, internal standard normalization of signals against endogenous homogeneously distributed elements has some utility. For example, carbon and phosphorus are abundant in biological tissues and often proportional to sample thickness for similar cell populations [9–13]. Carbon normalization was first proposed by Feldmann, Kindness and Ek [14] to correct variations of ablation efficiencies, absorption coefficients, and signal intensities, and has been shown to improve precision of elemental measurements across heterogeneous samples within constrained criteria [13,15]. However, later studies demonstrated that carbon produced matrix dependent reaction products upon ablation and was not viable for effective universal normalization [16,17]. Similarly, phosphorus may track cell tissue density under limited circumstances, and as with carbon, is not suitable as an internal standard across heterogeneous tissue sections where variations in elemental distributions do not correlate with structure or thickness.

Other internal standardization methods employ fabricated thin polymer films, placed under or on top of tissue sections, improving precision and accuracy by compensation of laser power variability and instrumental drift [7,12,18]. However, these approaches are not practicable for incorporation into routine analytical workflows due to increased sample preparation complexity, costs and time.

Regardless of the chosen quantification method, complete mitigation of tissue heterogeneity, differential shrinkage, cutting artefacts, and laser power variability remain unresolved. Recent advances and capital cost reductions of optical profilometry technologies provide a simple robust solution. Here, the specimen may be scanned to obtain detailed surface topography and tissue thickness maps prior to ablation, allowing volume normalization per voxel across the entire sample. The viability of volume normalization was recently demonstrated for selected regions of reference glass substrates of varying density [7].

Accordingly, we present the incorporation of optical profilometry into elemental bioimaging analytical workflows for concomitant measurements of specimen surface topography and thickness, and subsequent volume normalization for improved precision, accuracy and repeatable quantification of elemental distributions in a variety of tissues. We further evaluated the effectiveness of endogenous carbon and phosphorus for normalization of various tissue structures and cell populations.

2. Materials and methods

2.1. Chemicals and reagents

High-purity single-element standard calibration solutions of 1000 mg L^{-1} (Fe, Cu, and Zn) were purchased from Choice Analytical (Thornleigh, NSW, Australia). Ultrapure water (18.2 MΩ cm) was obtained from a Sartorius 611 Arium® Pro water generation system and used for all standard preparations. Ultrapure Nitric acid was supplied by Choice Analytical (Thornleigh, New South Wales, Australia). Xylene and ethanol were obtained from ChemSupply (Gillman, SA, Australia). HybriWell™ molds (9.8 mm × 20 mm × 0.16 mm) and high-purity porcine gelatin were obtained from Sigma-Aldrich.

2.2. Preparation of gelatin-based standards

Gelatin standards were prepared following protocols by Lockwood, Westerhausen and Doble [19]. Briefly, 83.3 mg of high-purity porcine gelatin was mixed with 917 µL Tris-HCl buffer (pH 7.4), 10 mM EDTA and 1 % w/w polyethylene glycol (M_n 400). UV absorbent additive gallic acid was added to the buffer at a concentration of 5 g L^{-1} before the addition of the buffer to the gelatin, corresponding to 1–5 % dry weight. This solution was spiked with various levels of Fe, Cu, and Zn, heated to 55 °C, and pipetted into HybriWell™ molds. The molds were frozen for 10 min at −80 °C, and dried at room temperature, producing uniform and smooth standards with expected thicknesses of 15 µm. The concentrations of each element in the gelatin standards were cross validated by acid digestion of dried gelatin, followed by triplicate measurements using solution nebulization ICP-MS [8].

Table 1
Operating conditions for the LA-ICP-MS.

Instrument Parameter	Setting
Laser MFC 1 and 2	0.5, 0.2 ml min^{-1} He
RF Power	1350 W
Plasma gas flow rate (L min^{-1})	15
Nebulizer Gas	0.45 L min^{-1}
Sample depth	5 mm
Extract lens 1 and 2	−2 V, −240 V
Omega bias and lens	−115 V, 7.5 V
Octopole bias and RF	−20V, 200V
Deflect	5 V
He Collision gas	3.0 min^{-1}
Isotopes	^{56}Fe,^{63}Cu,^{66}Zn,^{12}C,^{31}P

2.3. Microarrays and biological tissue sections

A formalin-fixed, paraffin-embedded (FFPE) multi-organ adjacent tissue microarray (BC001130s, Tissue Array, USA) containing carcinoma, normal, and adjacent normal tissues, was used for method development. Archived murine samples were obtained from the Garvan Institute of Medical Research-St Vincent's Hospital Ethics Committee (Ethical Approval No. 22_04). All tissue collections adhered to the Australian Code of Practice for the Care and Use of Animals for Scientific Purposes. Murine tissues were formalin-fixed in 4 % formaldehyde for 24 h before paraffin embedding using a Leica Peloris II tissue processor. Sections were cut at 5 µm, mounted on glass slides, and prepared for histological evaluation. Additional formalin-fixed, paraffin-embedded human tissue samples were also retrieved from the anonymized archives of the Institute of Neuropathology at University Hospital Münster, Germany (Ethical Approval 1IIIPau). Sections were cut at 30 µm, mounted on glass slides, and evaluated histologically by a certified neuropathologist. Prior to optical profilometry and LA-ICP-MS analyses, the microarrays and tissue sections were deparaffinized using xylene and ethanol, following previously established protocols [8]. Histological image processing was performed using QuPath software.

2.4. LA-ICP-MS measurements

Elemental images were acquired using an ESL imageBIO266 (Kenelec Scientific, Mitcham, Australia) equipped with a TwoVol3 ablation chamber, coupled to an Agilent 7900 ICP-MS (Agilent Technologies, Santa Clara, CA, USA). Helium (He) was used as carrier gas (99.999 % purity, BOC, North Ryde, NSW, Australia).

Elemental images and corresponding calibration standards were acquired using a 30 µm (laser spot size at 200 Hz and a scan speed of 300 µm s^{-1} for the meningioma, and a 20 µm laser spot size at 200 Hz with a scan speed of 200 µm s^{-1} for the kidney. The ICP-MS instrument was tuned for maximum sensitivity before each measurement using NIST 612 glass CRM. Isotope ratios Ce/CeO were monitored to confirm the absence of interfering polyatomic species. The total integration time of all elements for each quadrupole sweep was 0.1 s to produce square image voxels that maintained relative specimen image dimensions. Pew2 v 1.7.0 was used for image reconstruction.[20] Typical instrument

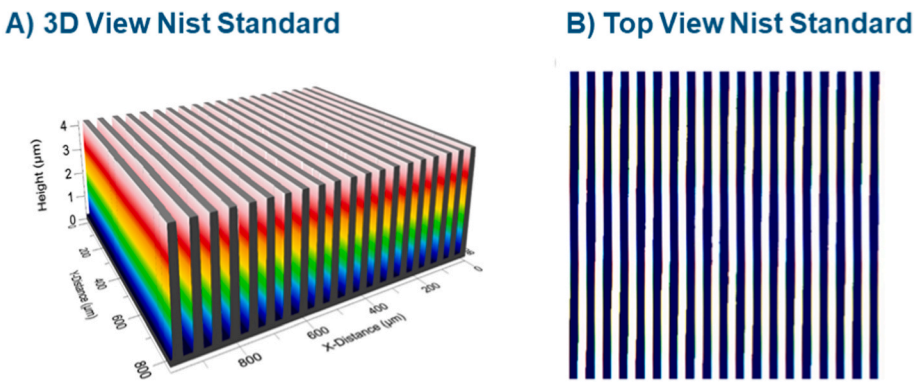

Fig. 1. Calibration of the 3D Optical Profiler using the 4 µm NIST "Multi-Step: Step-Height Standard" reference substrate. (A) 3D view and (B) top view of post-calibration scanning of the NIST reference substrate demonstrating suitability of the optical profilometer for measurements of surface topography and thickness of typical biological specimens in routine analytical imaging workflows.

Table 2
Hardware and software operating conditions for the Filmetrics Profilm 3D Optical Profilometer.

Instrument Parameter	Setting
Piezoelectric Voltages 1; 2 and 3	29; 30; 29 V
Vibration Amplitude	Less than 0.01 nm
Original Intensity Slice (Horizontal and Vertical)	200 pixels
Magnification lens and zoom	20x; 2x
Tilt (number of fringes)	2
Measurement	Green Light Interferometry (GLI)
Light Source Intensity	70 mW. cm-^{2}
GLI settings	Envelop peak; top layer; 1.5 % threshold
Back Scan; Scan Length	0.01; 0.04 mm (variable)
Scan Speed	Normal
Pixel Area	1

parameters are outlined in Table 1.

2.4.1. LA-ICP-MS calibration

Calibration curves were constructed by plotting average signal intensities of each element against concentration (ug g^{-1}) from 5 individual ablation lines of each standard. Conversions to mass/volume concentrations (ug cm^{-3}) were performed by consideration of reported nominal thickness and profile normalization of each voxel [5,18] (Supplementary Note S1). The entire tissue was completely removed in all samples for direct comparisons between nominal and volume corrected distributions.

2.5. Calibration and 3D optical profilometer measurement

A Filmetrics Profilm 3D (Warsash Scientific; Redfern, Australia) was used to acquire detailed surface topography and thickness characterizations of representative tissue specimens on glass slides and gelatin-based standards. The 3D Optical Profiler was calibrated according to the manufacturer's specifications via scanning a Multi-Step: Step-Height Standard reference substrate (Reference number SHS-16205). The calibration produced step heights that were within 0.08 % (1 nm) of the certified reference values, well within the manufacturer's tolerance specification (Fig. 1).

Greenlight interferometry was chosen for profiling, as it allowed sufficient penetration of photons to reduce unwanted light scattering and minimization of chromatic aberrations, resulting in clearer interference patterns and optimal measurements for both the tissues and gelatin standards [20]. Typical instrument parameters are outlined in Table 2.

Surface topography and thickness were measured with 20 × magnification, representing an x, y image resolution of 3.48 µm^{2} per voxel. Ten consecutive measurements were taken across each tissue in increments of 2.0 × 2.0 mm^{2} producing valid voxels for 98 % of each specimen, and surface topography measurements with a maximum of 0.5 nm variability (RSD). Once the scan was completed, the Filmetrics Profilm 3D software was used to integrate the images. The remaining 4 % of invalid pixels were interpolated using the Clough-Tocher cubic algorithm.

2.6. Data acquisition and processing

Surface profiles and topographies were processed using Profilm Optical Profiler software (version 4.3.8.0). The proprietary Filmetrics Binary (.fibps) files were exported as comma separated values (.csv) and imported into Pew^{2} v1.7.0 and Paraview (5.13.3), open-source imaging software, to reconstruct high-resolution topographic maps [19]. The topography data was down-sampled using averaging to match the voxel size of the LA-ICP-MS elemental images and both sets of data were registered via Fourier transform domains and cross correlations for both translational and rotational offsets. Asymptotic two-sided Mann-Whitney U tests with tie correction were applied to evaluate significant differences in ablation volume [18]. Volumetric measurements of ablated craters were cross-validated in our previous study by comparing profilometer outputs with non-contact atomic force microscopy (NC-AFM) across different spot sizes and laser fluences, confirming no significant differences in crater volumes (Mann–Whitney U, $p = 0.62$). These results support the robustness of the profilometry-based volumetric approach applied in this work [29].

2.7. Measurements of cell density

Cell density maps were constructed from a hematoxylin and eosin (H&E) consecutive stained section of a human meningioma, digitized using a Zeiss Axioscan7 slide scanner (20 × magnification, 0.22 µm pixel size; Macquarie Park, Australia). After loading the image into QuPath 0.6.0-rc3, cells were detected using the native QuPath algorithm with default parameters [21]. Cell density maps were then produced using a density radius of 30 µm, exported, down sampled and registered with the LA-ICP-MS images, as described above.

2.8. Image construction

All processed data were formatted as Visualization Toolkit files (.vtk and.vti) and images generated in Paraview (5.13.3). The Visualization Toolkit data files are available for download in Supplementary Materials.

Table 3
Comparison of nominal microtome cutting nominal thickness, actual thickness, surface roughness and profilometric characterization of tissue surfaces.

Sample	Nominal thickness (μm)	Measured Thickness (μm)						
		Maximum	Minimum	Mean	Arithmetic mean (Sa)[a]	Root mean square (Sq)[a]	Skewness (Ssk)[a]	Kurtosis (Sku)[a]
Gelatin standards	15	13.2	11.8	12.5	0.09	0.12	−0.05	3.4
Multi-organ Microarrays	5	9.4	2.3	2.8	0.3	0.5	2.8	15.0
Murine Kidney tissue	5	7.0	1.7	2.5	0.6	0.6	0.7	3.4
Human meningioma tissue	10	38.2	0.6	3.80	2.0	1.6	1.4	8.2
Emphysematous Murine Lung tissue	60	65.0	15.0	19.0	6.8	8.1	1.3	4.2

[a] Profilometric parameters that measure surface roughness include arithmetic mean height (*Sa*), root mean square height (*Sq*), skewness (*Ssk*), and kurtosis (*Sku*). *Sa* provides the average deviation of surface heights from a reference plane, representing overall surface roughness. *Sq* measures the root mean square of these deviations, offering a more sensitive indication of surface variation compared to *Sa*. *Ssk* describes asymmetry of height distributions, while *Sku* assesses sharpness or flatness of the surface.

Table 4
Comparison of elemental concentrations in murine kidney and human meningioma tissue samples using three quantification approaches: (1) standard quantification (non-normalized, μg g^{-1}), (2) ablation-volume correction based on nominal tissue thickness, and (3) ablation-volume correction using profile-derived data with volume normalization (μg cm^{-3}). Concentrations are presented based on tissue and gelatin density of 1.35 g cm^{-3}.

Element	Tissue Type/ Area	Maximum			Mean		
		Non-normalized (μg g^{-1})	Nominal Ablation-volume corrected (μg cm^{-3})	Profile Ablation-volume corrected (μg cm^{-3})	Non-normalized (μg g^{-1})	Nominal Ablation-volume corrected (μg cm^{-3})	Profile Ablation-volume corrected (μg cm^{-3})
^{56}Fe	Murine	660.03	1242.01	8325.83	44.02	153.13	700.03
^{63}Cu	Kidney	40.62	83.97	544.26	3.04	9.20	52.06
^{66}Zn		593.14	885.42	4863.56	30.03	66.01	282.13
^{56}Fe	Meningioma	4131.05	15128.05	14642.10	81.43	106.86	377.36
^{63}Cu	Whole tissue	239.02	390.03	1355.02	1.96	2.59	10.07
^{66}Zn		179.87	222.14	1714.04	5.80	6.16	64.11
^{56}Fe	Tumor area	774.01	2574.85	11051.33	130.21	159.05	718.57
^{63}Cu		8.98	18.04	79.42	1.35	1.62	8.85
^{66}Zn		84.62	98.82	512.88	12.23	13.05	108.58
^{56}Fe	Stroma area	4131.04	15127.07	10268.81	42.52	53.93	127.32
^{63}Cu		238.96	389.34	585.07	1.21	1.45	6.03
^{66}Zn		171.03	201.96	526.23	0.02	1.77	30.61

3. Results and discussion

3.1. Surface topography

Gelatin standards, as well as selected representative tissue sections comprising of multi-tissue microarrays, murine kidneys, and human meningioma were obtained from commercial and research sources, cut at various nominal thicknesses, and were scanned by optical profilometry. The surface topography was characterized by measurement of minimum, maximum and mean thickness and surface roughness descriptors as detailed by ISO 25178 [22,23]. These parameters were arithmetic mean height (*Sa*), root mean square height (*Sq*), skewness (*Ssk*), and kurtosis (*Sku*), and are presented in Table 3.

The gelatin standards expected nominal thickness of 15 μm mean value was measured at 12.5 ± 0.7 μm, with surface roughness descriptors indicating near-symmetric height distributions and moderately peaked profiles at the peripheries (see Table 4). These data describe a smooth and consistent surface with high uniformity, demonstrating preparation of precise and repeatable standards suitable for calibration and quantification of bioimaging workflows.

All representative tissue sections had intra-tissue surface topography variability and discordance of expected nominal thicknesses. The multi-organ microarrays used in this study included tissues from the eye, esophagus, lung, and brain (Figure S2 A-D), with nominal section thicknesses of 5 μm, according to the supplier's specifications. However, our measurements of mean thicknesses of 2.8 ± 0.5 μm deviated by approximately 45 %. High values of *Ssk* (2.8) and *Sku* (15.0) indicated significant surface asymmetry and large surface roughness variations. These irregularities were likely due to variations of cell populations, non-uniform sectioning, mechanical sheer or sectioning artefacts, and were unavoidable due to physical properties of disparate tissue structures [23].

The healthy murine kidney presented mean thickness of 2.5 μm ± 0.5 μm (nominally 5 μm). Surface roughness parameters of *Sa* = 0.6, *Sq* = 0.7, *Ssk* = 0.7, and *Sku* 3.4 indicated a moderately smooth surface with mild asymmetry, likely due to natural biological homogeneity [24].

The most pronounced discrepancies were observed in human meningiomas and emphysematous murine lung tissue. Despite an expected nominal cutting thickness of 10 μm, the meningioma's mean thickness was 3.80 μm, over 60 % less than expected. Surface roughness metrics (*Sa* 2.0; *Sq* 1.6) and elevated *Ssk* (1.4) and *Sku* (8.2) highlight significant irregularity. These findings were consistent with the known cellular compositions of varying densities, and tightly packed spindle-shaped cells within collagen-rich extracellular matrices. These features contribute to tissue rigidity and anisotropic deformation during embedding and sectioning, particularly for fibrous and transitional tissue structures, likely amplifying average thickness variance due to resistance to compression, and interactions with the microtome blade [25].

The emphysematous murine lung tissue section (Fig. S2E) exhibited the greatest variability, with average thicknesses of 19.0 μm (nominal: 60 μm), ranging from 15.0 to 65.0 μm. This sample had the highest roughness values (*Sa* 6.8; *Sq* 8.1), indicating significant surface irregularities. Skewness (*Ssk* = 1.3) and kurtosis (*Sku* = 4.2) indicated asymmetric height distribution with moderately sharp tissue peaks, likely attributable to the fragile and porous nature of emphysematous tissue,

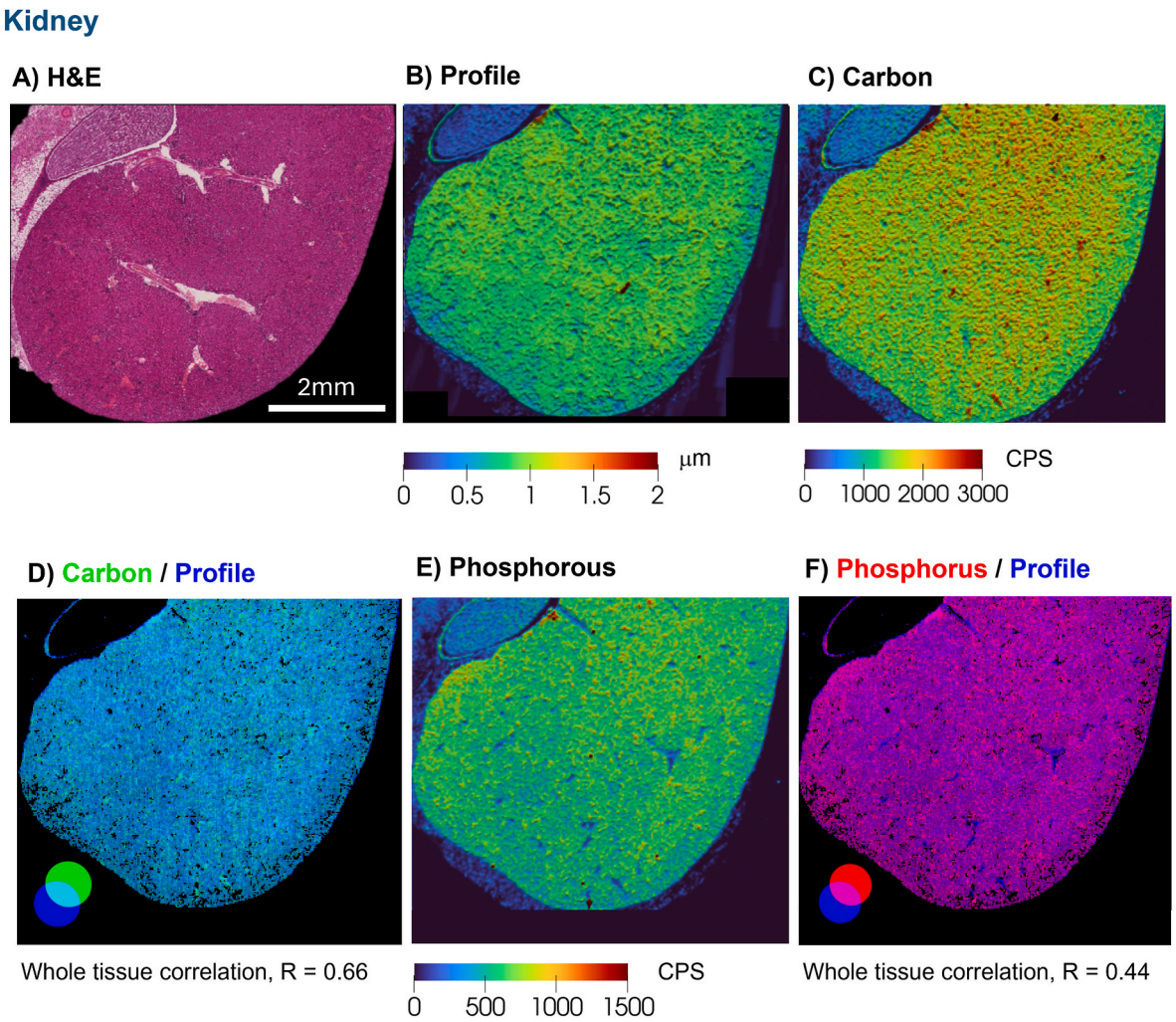

Fig. 2. Correlations of profile, ^{12}C and ^{31}P in a healthy murine kidney. A) Hematoxylin and eosin staining; B) Tissue topography measured by optical profilometry (nominal thickness 5 µm); C) ^{12}C (CPS); D) Whole tissue correlation of ^{12}C and profile, E) ^{31}P (CPS); and F) Whole tissue correlation of ^{31}P and profile.

with greater surface irregularity and heterogeneity compared to other tissue types [26].

These results demonstrate that surface topology and sample thicknesses were dependent upon tissue composition, sample processing methods and/or physical forces during sectioning. Shrinkage, anisotropic deformation, variations induced by embedding media, microtome blade mechanics, and tissue hydration may also contribute to these inconsistencies. For example, tissue shrinkage, often driven by dehydration and fixation, may lead to a 50 % volumetric reduction, with more pronounced deformation along the z-axis due to compression during sectioning [27]. These results challenge the assumption of flat and homogeneous tissue sections, necessitating considerations of surface topography for all imaging workflows to ensure correct interpretation of elemental distributions. For example, non-uniform thickness and surface roughness may disrupt laser-tissue coupling, adversely affecting ablation and detector responses that may introduce bias, potentially compromising accuracy and reproducibility of analyses. It is also important to note that sample preparation procedures, such as deparaffinization, could alter tissue composition by extracting or redistributing soluble species, meaning absolute concentrations may differ from untreated (fresh-frozen) samples [28]. Nevertheless, the optical profilometry–based correction introduced here addresses volumetric artefacts rather than analyte recovery and is therefore applicable to both paraffin-embedded and fresh-frozen tissues. Integration of profilometric measurements and volume-corrected signal normalization is therefore necessary for accurate quantification, particularly in longitudinal studies [29].

3.2. *Correlations of carbon and phosphorus with tissue thickness and cell density*

We assessed the correlation of ^{12}C and ^{31}P signal intensities and tissue surface topography of two morphologically distinct tissue types, i.e., the homogenous murine kidney and the heterogeneous human meningioma, using integrated surface profilometry and elemental bioimaging (Figs. 2 and 3). The murine kidney tissue section had a strong positive correlation ($R = 0.66$) between ^{12}C and surface topography (Fig. 2D), demonstrating that ^{12}C closely tracked tissue thickness. In contrast, the correlation between ^{31}P and surface topography ($R = 0.44$) was moderate (Fig. 2F), indicating that phosphorus was not related to the physical thickness of the tissue section despite its uniform structure. This moderate correlation implied that the ^{31}P distribution was likely governed by biological variability such as localized cell density or organelle content.

The correlation between ^{12}C and surface topography ($R = 0.21$) of the heterogenous meningioma was tenuous (Fig. 3E). This poor correlation was consistent with literature reports that carbon distributions are dependent upon specimen hydration, background atmospheric carbon, argon carrier gas impurities and matrix-dependent partitioning of gaseous and particulate phases during ablation. These aspects were not

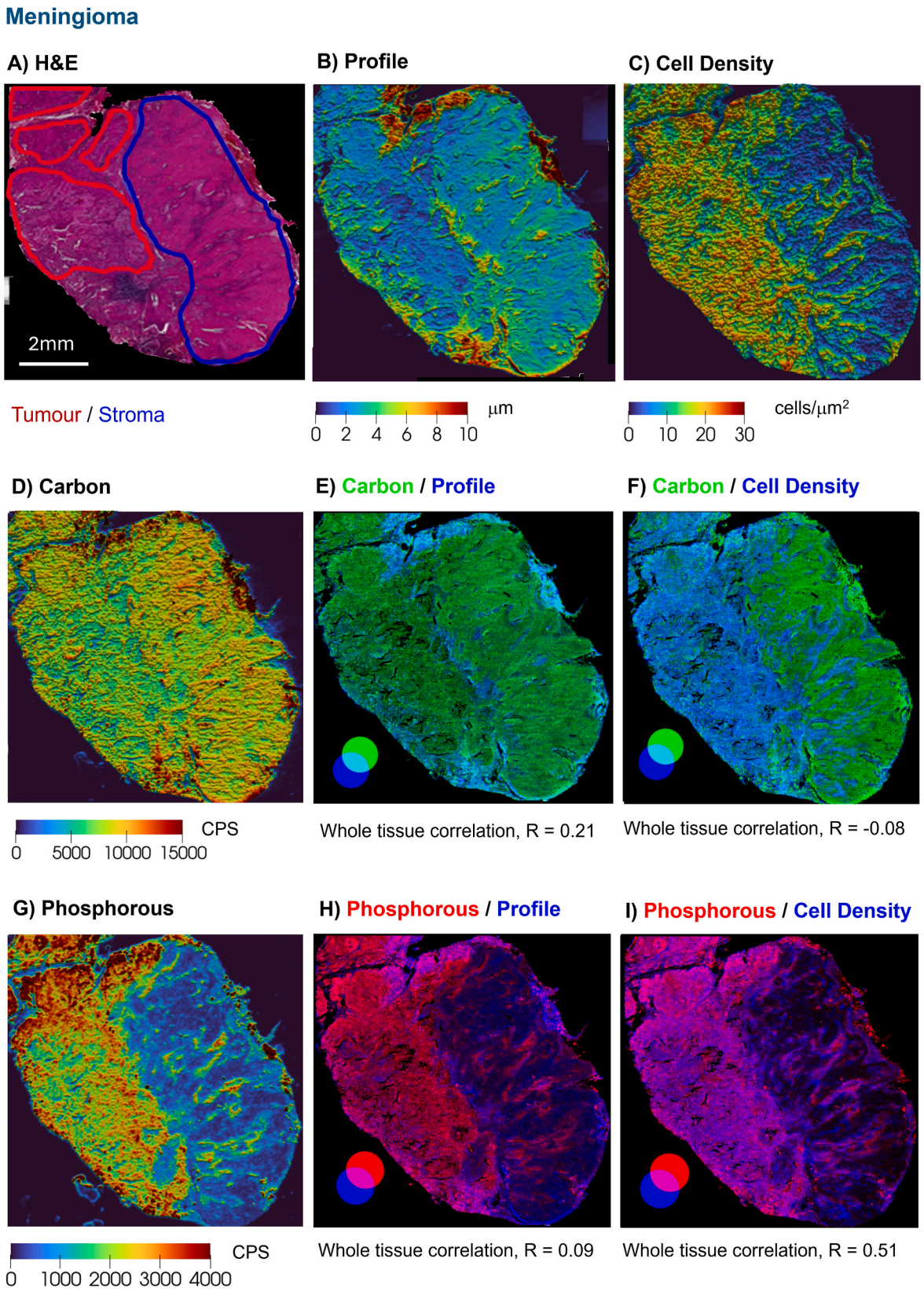

Fig. 3. Correlations of profile and ^{12}C and ^{31}P in a human meningioma. A) Hematoxylin and eosin staining, tumorous regions outlined in red and stroma in blue; B) Tissue topography measured by optical profilometry (nominal thickness 10 µm); C) Cell density (cells μm^{-2}, D) ^{12}C (CPS); E) Whole tissue correlation of ^{12}C and profile, F) Whole tissue correlation of ^{12}C and cell density; G) ^{31}P (CPS); H) Whole tissue correlation of ^{31}P and profile; and I) Whole tissue correlation of ^{31}P and cell density. (For interpretation of the references to colour in this figure legend, the reader is referred to the Web version of this article.)

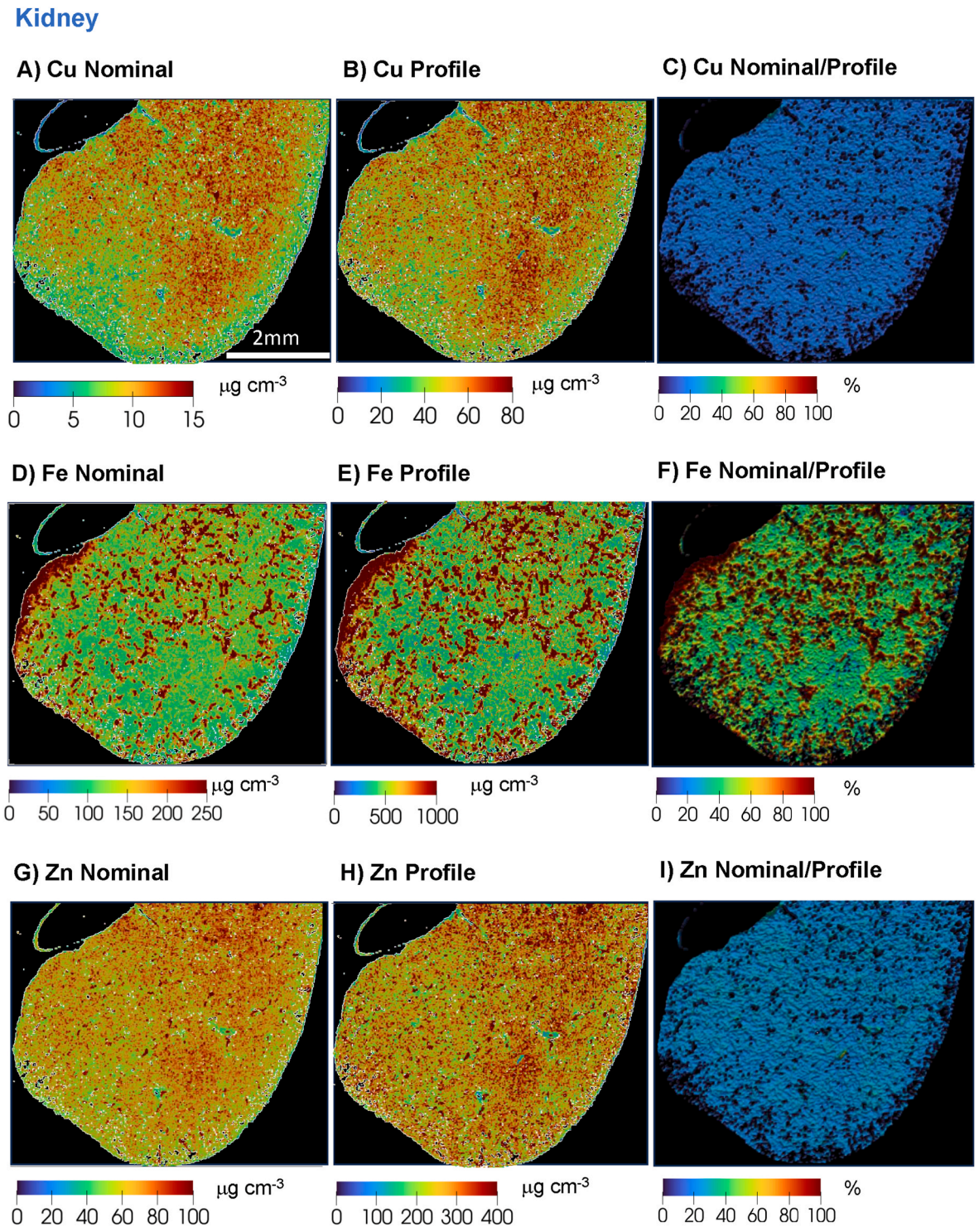

Fig. 4. Volume correction of murine kidney with optical profilometry. A) Cu volume concentration (µg cm^{-3}) based on nominal thickness (5 µm); B) Cu profile volume correction (µg cm^{-3}) by optical profilometry); C) Cu % change of nominal thickness/profile corrected; D) Fe volume concentration (µg cm^{-3}) based on nominal thickness (5 µm); E) Fe profile volume correction (µg cm^{-3}) by optical profilometry); F) Fe % change of nominal thickness/profile corrected; G) Zn volume concentration (µg cm^{-3}) based on nominal thickness (5 µm) H) Zn profile volume correction (µg cm^{-3}) by optical profilometry); I) Zn % change of nominal thickness/profile corrected.

apparent with the uniform kidney section; however, our results confirm that carbon normalization has limited utility as a universal internal standard across structurally diverse biological specimens. There was no correlation between ^{31}P and surface topography (R = 0.09) (Fig. 3H). While phosphorus is a major constituent of nucleic acids and phospholipid membranes, its spatial distribution is strongly influenced by cellular composition, metabolic activity, and tissue architecture. Additionally, phosphate-binding proteins and compartmentalization of phosphorus-rich organelles likely contribute to signal variability independent of thickness [30].

We also compared correlations of cell density and profile with ^{12}C and ^{31}P in the meningioma section. The correlation between ^{12}C and cell

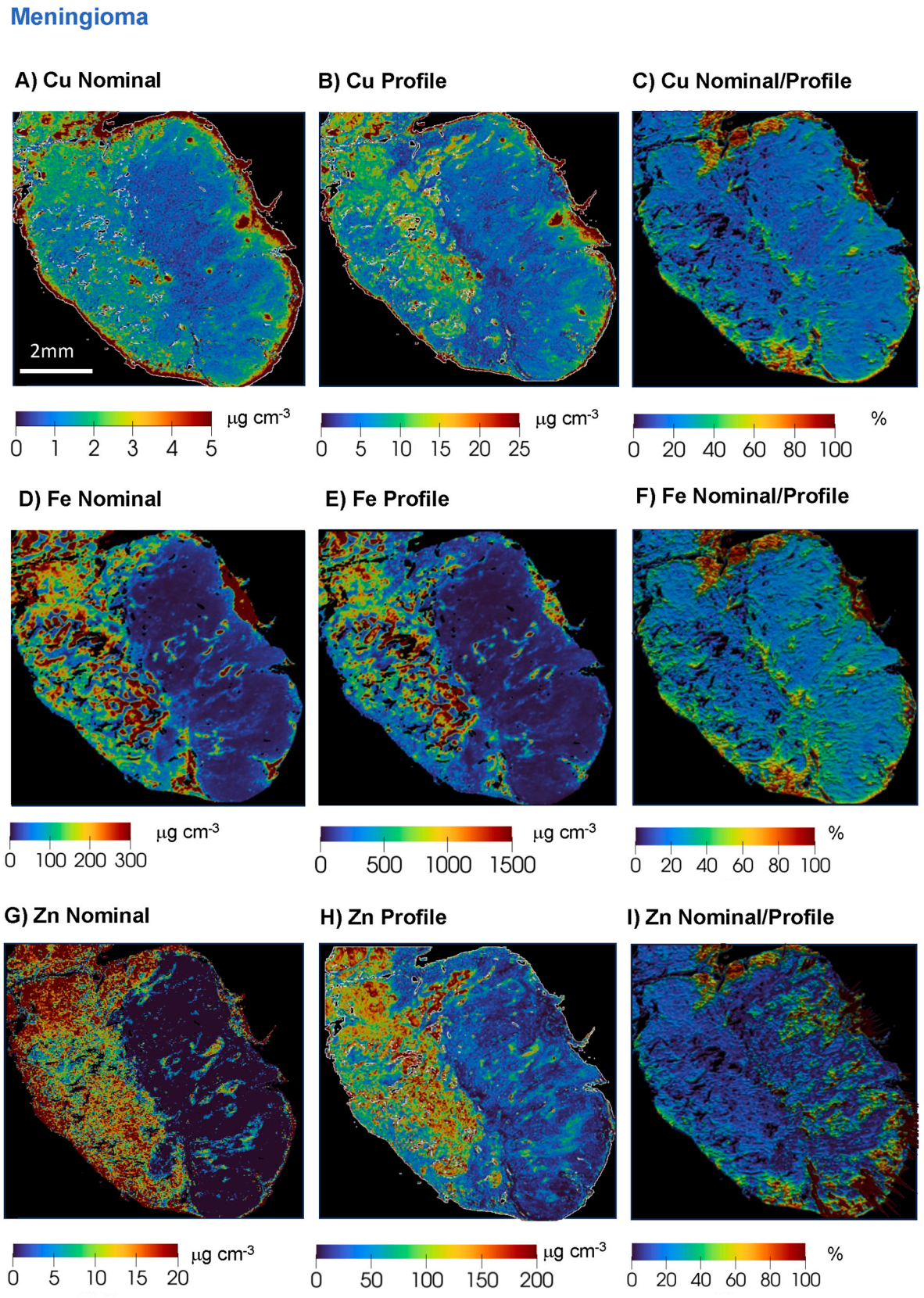

Fig. 5. Volume correction of meningioma with optical profilometry. A) Cu volume concentration (μg cm^{-3}) based on nominal thickness (10 μm); B) Cu profile volume correction (μg cm^{-3}) by optical profilometry); C) Cu % change of nominal thickness/profile corrected; D) Fe volume concentration (μg cm^{-3}) based on nominal thickness (5 μm); E) Fe profile volume correction (μg cm^{-3}) by optical profilometry); F) Fe % change of nominal thickness/profile corrected; G) Zn volume concentration (μg cm^{-3}) based on nominal thickness (5 μm) H) Zn profile volume correction (μg cm^{-3}) by optical profilometry); I) Zn % change of nominal thickness/profile corrected.

density was negligible (R = −0.08) (Fig. 3F), demonstrating that carbon was not associated with cellular architecture. In contrast, ^{31}P showed moderate correlation (R = 0.51) with cellular density (Fig. 3I). Regardless, the disparate distributions of both ^{12}C and ^{31}P between tumourous areas (marked in red) and stroma (blue) tissue (Fig. 3 A) may have some utility for examination of cancers, for example, identification of tumor boundaries and precancerous cell populations that are not visible with H&E staining [31].

3.3. Volume-corrected surface quantification of essential elements in tissues

These profilometry analyses have major implications when elemental bioimaging quantification relies solely upon reported nominal microtome thickness, particularly for heterogeneous tissues such as meningiomas and emphysematous lungs. Accordingly, we applied volume correction to two representative tissue sections (murine kidney and human meningioma), using surface topography measurements and nominal tissue thickness. This required surface characterization by optical profilometry of the gelatin calibration standards pre- and post-ablation (Fig. S1). Visual inspection of the samples post-ablation revealed complete removal of tissues from the glass substrate after analysis.

The murine kidney had relatively smooth surface topography, uniform sample thickness and homogeneous cell populations. Profile-volume correction resulted in a 4-to-5-fold increase of measured elemental concentrations, as illustrated in Fig. 4. Scaled quantified images of Cu, Fe and Zn appear near identical with the same structural features of all elements across the tissue. However, each element's concentration distributions changed differently, illustrated by nominal thickness/profile percent ratios. Cu was consistently 15 to 20 % of volume corrected concentrations across the tissue (Fig. 4C), and Zn was consistently 20 to 30 % across the tissue (Fig. 4I). These data indicated that the uniform surface topography and sample thickness provided reliable relative quantification with or without volume correction for Cu and Zn, albeit with marked changes of absolute values. However, this example was a rare exception as most tissues have considerable thickness and surface profile irregularities [27]. In contrast, Fe ranged from approximately 20 to 100 %, with the higher values tracking the pronounced vascular structural features within the kidney (Fig. 4F), highlighting potential misleading interpretations of standard quantification approaches.

The relative differences of elemental distributions obtained by nominal and profile volume corrections in the human meningioma specimen were significant (Fig. 5). Volume correction uniformly increased the concentration of Cu (Fig. 5C) and Fe (Fig. 5F) by approximately 8 to 10 times in both the stroma and tumourous areas when viewed as nominal thickness/profile percent ratios. Similar increases of Zn (Fig. 5I) were observed in areas within the stroma; however, the distribution of these changes were more frequent when compared to Cu and Fe. The significant changes of volume normalized concentrations of all elements indicate that distributions were dependent upon tissue type, densities, laser coupling efficiencies, and other factors.

These data clearly show that characterization of specimen thickness is necessary for reliable quantification as all evaluated tissues were not concordant with expected nominal thickness. Although relative quantification trends were similar for healthy tissues with uniformly cut sections and similar cell populations, dramatic changes were observed when the specimen consisted of domains of disparate cell populations with various regions of interest increasing or decreasing by at least an order of magnitude.Therefore, volume normalization is an essential requirement for comparative longitudinal studies to ensure appropriate interpretation and valid conclusions of elemental changes in biological studies.

4. Conclusion

Incorporation of optical profilometry into quantitative elemental bioimaging workflows is required to correct tissue thickness variations, cryotome cutting artefacts, and matrix-dependent ablation anomalies. Consistent trends of relative elemental distributions of nominal and profile volume corrected measurements were observed in murine kidney with similar cell populations, where Cu and Zn measured values uniformly increased by approximately 4 to 5-fold, however Fe concentrations were more variable. Profile correction of Cu, Fe and Zn in the heterogeneous meningioma increased by up to 10-fold and were not uniformly observed across the tissue.

Our results confirm that endogenous internal standards, such as carbon and phosphorus, were inadequate for correction of thickness variability for heterogeneous tissues and offer limited utility for uniformly sectioned tissues with similar cell populations and densities.

Incorporation of surface topography metrics is essential to improve precision, accuracy, and reproducibility of elemental bioimaging. Optical profilometry overcomes the final limitation of quantification workflows associated with variable tissue thicknesses that have obscured observation and understanding of subtle changes of elemental interactions by effectively mitigating inter- and intra-sample variabilities and measurement biases in healthy and diseased tissues. While the correction process improved data quality, whole tissue topographic measurements increased total analysis time. This may limit scalability for studies involving large cohorts; however, automation or selection of smaller regions of interest will facilitate integration of surface topography correction into routine analytical workflows, allowing transformative applications of imaging mass spectrometry.

CRediT authorship contribution statement

Dayanne Mozaner Bordin: Writing – review & editing, Writing – original draft, Methodology, Investigation, Formal analysis, Conceptualization. **Thomas Lockwood:** Writing – original draft, Visualization, Software, Methodology, Formal analysis. **Mika Westerhausen:** Investigation. **Janice Irene McCauley:** Writing – original draft. **Astrid Jeibmann:** Writing – original draft, Project administration. **Jessica Chitty:** Writing – review & editing, Writing – original draft, Resources. **Thomas Cox:** Writing – review & editing, Writing – original draft, Resources. **Philip A. Doble:** Writing – review & editing, Writing – original draft, Resources, Methodology, Investigation, Funding acquisition, Formal analysis, Conceptualization.

Declaration of competing interest

The authors declare the following financial interests/personal relationships which may be considered as potential competing interests:

Dayanne Cristiane Mozaner Bordin reports financial support was provided by Philanthropic support from the Mikos Family. Philip Doble reports financial support was provided by Philanthropic support from the Mikos Family. Janice Irene McCauley reports financial support was provided by Philanthropic support from the Mikos Family. Thomas Cox reports financial support was provided by National Health and Medical Research Council. Thomas Cox reports financial support was provided by Cancer Council New South Wales. Jessica Chitty reports financial support was provided by National Health and Medical Research Council. Jessica Chitty reports financial support was provided by Cancer Council New South Wales. If there are other authors, they declare that they have no known competing financial interests or personal relationships that could have appeared to influence the work reported in this paper.

Acknowledgements

DMB, PAD and JIM gratefully acknowledge the philanthropic support from the Mikos Family. TRC and JC are supported by the NHMRC

(2033065, 1158590) and CCNSW (19-09, 21-11).

Appendix A. Supplementary data

Supplementary data to this article can be found online at https://doi.org/10.1016/j.talanta.2025.128923.

Data availability

Data will be made available on request.

References

[1] D. Pozebon, G.L. Scheffler, V.L. Dressler, Recent applications of laser ablation inductively coupled plasma mass spectrometry (LA-ICP-MS) for biological sample analysis: a follow-up review, J. Anal. At. Spectrom. 32 (5) (2017) 890–919.

[2] P.A. Doble, R.G. de Vega, D.P. Bishop, D.J. Hare, D. Clases, Laser ablation-inductively coupled plasma-mass spectrometry imaging in biology, Chem. Rev. 121 (19) (2021) 11769–11822.

[3] J. Lear, D. Hare, P. Adlard, D. Finkelstein, P. Doble, Improving acquisition times of elemental bio-imaging for quadrupole-based LA-ICP-MS, J. Anal. At. Spectrom. 27 (1) (2012) 159–164.

[4] M.G. Mello, T.E. Lockwood, J. Wanagat, M.T. Westerhausen, D.P. Bishop, Improvement in the sensitivity of LA-ICP-MS bioimaging by addition of nitrogen to the argon carrier gas, J. Anal. At. Spectrom. 39 (7) (2024) 1720–1725.

[5] K. Mervič, M. Šala, S. Theiner, Calibration approaches in laser ablation inductively coupled plasma mass spectrometry for bioimaging applications, TrAC Trends Anal. Chem. (Reference Ed.) 172 (2024).

[6] P.A. Doble, G.L.G. Miklos, Distributions of manganese in diverse human cancers provide insights into tumour radioresistance, Metallomics 10 (9) (2018) 1191–1210.

[7] K. Mervic, V.S. Selih, M. Sala, J.T. van Elteren, Non-matrix-matched calibration in bulk multi-element laser ablation - inductively coupled plasma - mass spectrometry analysis of diverse materials, Talanta 271 (2024) 125712.

[8] M.T. Westerhausen, T.E. Lockwood, R. Gonzalez de Vega, A. Röhnelt, D.P. Bishop, N. Cole, P.A. Doble, D. Clases, Low background mould-prepared gelatine standards for reproducible quantification in elemental bio-imaging, Analyst 144 (23) (2019) 6881–6888.

[9] M. Aramendía, L. Rello, S. Bérail, A. Donnard, C. Pécheyran, M. Resano, Direct analysis of dried blood spots by femtosecond-laser ablation-inductively coupled plasma-mass spectrometry. Feasibility of split-flow laser ablation for simultaneous trace element and isotopic analysis, J. Anal. At. Spectrom. 30 (1) (2015) 296–309.

[10] A. Arakawa, N. Jakubowski, G. Koellensperger, S. Theiner, A. Schweikert, S. Flemig, D. Iwahata, H. Traub, T. Hirata, Quantitative imaging of silver nanoparticles and essential elements in thin sections of fibroblast multicellular spheroids by high resolution laser ablation inductively coupled plasma time-of-flight mass spectrometry, Anal. Chem. 91 (15) (2019) 10197–10203.

[11] D. Drescher, C. Giesen, H. Traub, U. Panne, J. Kneipp, N. Jakubowski, Quantitative imaging of gold and silver nanoparticles in single eukaryotic cells by laser ablation ICP-MS, Anal. Chem. 84 (22) (2012) 9684–9688.

[12] C. Austin, D. Hare, T. Rawling, A.M. McDonagh, P. Doble, Quantification method for elemental bio-imaging by LA-ICP-MS using metal spiked PMMA films, J. Anal. At. Spectrom. 25 (5) (2010).

[13] A. Limbeck, P. Galler, M. Bonta, G. Bauer, W. Nischkauer, F. Vanhaecke, Recent advances in quantitative LA-ICP-MS analysis: challenges and solutions in the life sciences and environmental chemistry, Anal. Bioanal. Chem. 407 (22) (2015) 6593–6617.

[14] J. Feldmann, A. Kindness, P. Ek, Laser ablation of soft tissue using a cyrogenically cooled ablation cell, J. Anal. At. Spectrom. 17 (8) (2002) 813–818.

[15] C. Austin, F. Fryer, J. Lear, D. Bishop, D. Hare, T. Rawling, L. Kirkup, A. McDonagh, P. Doble, Factors affecting internal standard selection for quantitative elemental bio-imaging of soft tissues by LA-ICP-MS, J. Anal. At. Spectrom. 26 (7) (2011).

[16] J.-L. Todoli, J.-M. Mermet, Study of polymer ablation products obtained by ultraviolet laser ablation -inductively coupled plasma atomic emission spectrometry, Spectrochim. Acta, Part B 53 (1998) 1645–1656.

[17] D.A. Frick, D. Günther, Fundamental studies on the ablation behaviour of carbon in LA-ICP-MS with respect to the suitability as internal standard, J. Anal. At. Spectrom. 27 (8) (2012).

[18] K. Mervic, J.T. van Elteren, M. Bele, M. Sala, Utilizing ablation volume for calibration in LA-ICP-MS mapping to address variations in ablation rates within and between matrices, Talanta 269 (2024) 125379.

[19] T.E. Lockwood, M.T. Westerhausen, P.A. Doble, Pew2: open-source imaging software for laser ablation-inductively coupled plasma-mass spectrometry, Anal. Chem. 93 (30) (2021) 10418–10423.

[20] L. Tonietto, D.C.M. Arnold, V.C. de Oliveira, C.W. Menegotto, A.E.B. Grondona, C. A.D. Costa, M.R. Veronez, C. de Souza Kazmierczak, L. Gonzaga Jr., Method for evaluating roughness and valley areas coefficients of surfaces acquired by laser scanner, Sci. Rep. 12 (1) (2022) 1486.

[21] P. Bankhead, M.B. Loughrey, J.A. Fernandez, Y. Dombrowski, D.G. McArt, P. D. Dunne, S. McQuaid, R.T. Gray, L.J. Murray, H.G. Coleman, J.A. James, M. Salto-Tellez, P.W. Hamilton, QuPath: open source software for digital pathology image analysis, Sci. Rep. 7 (1) (2017) 16878.

[22] I. 25178-2, ISO 25178-2:2021(en) Geometrical Product Specifications (GPS) — Surface Texture: Areal — Part 2: Terms, Definitions and Surface Texture Parameters, 2021.

[23] K. Singh, N. Paliwal, K. Kasamias, Surface roughness characterization using representative elementary area (REA) analysis, Sci. Rep. 14 (1) (2024) 1785.

[24] I.V. Murray, M.A. Paolini, Histology, Kidney and Glomerulus, StatPearls Publishing, 2023.

[25] R.A. Buerki, C. Horbinski, T. Kruser, P.M. Horowitz, C.D. James, R.V. Lukas, An overview of meniongiomas, Future Oncol. 14 (21) (2018) 2161–2177.

[26] Y.S. Khan, D.T. Lynch, Histology, Lung, StatPearls Publishing, 2023.

[27] K.A. Dorph-Petersen, J.R. Nyengaard, H.J. Gundersen, Tissue shrinkage and unbiased stereological estimation of particle number and size, J. Microsc. 204 (Pt 3) (2001) 232–246.

[28] M. Bonta, S. Torok, B. Hegedus, B. Dome, A. Limbeck, A comparison of sample preparation strategies for biological tissues and subsequent trace element analysis using LA-ICP-MS, Anal. Bioanal. Chem. 409 (7) (2017) 1805–1814.

[29] T.E. Lockwood, D.C.M. Bordin, M.T. Westerhausen, D.P. Bishop, Preparation of gelatine calibration standards for LA-ICP-MS bioimaging with 266 nm laser ablation systems, Talanta 283 (2025) 127150.

[30] L. Mueller, A.J. Herrmann, S. Techritz, U. Panne, N. Jakubowski, Quantitative characterization of single cells by use of immunocytochemistry combined with multiplex LA-ICP-MS, Anal. Bioanal. Chem. 409 (14) (2017) 3667–3676.

[31] D. Hare, F. Burger, C. Austin, F. Fryer, R. Grimm, B. Reedy, R.A. Scolyer, J. F. Thompson, P. Doble, Elemental bio-imaging of melanoma in lymph node biopsies, Analyst 134 (3) (2009) 450–453.